Journal of Power Sources 245 (2014) 352–361

Contents lists available at SciVerse ScienceDirect

Journal of Power Sources

journal homepage: www.elsevier.com/locate/jpowsour

Comparative study of $CoFeN_x/C$ catalyst obtained by pyrolysis of hemin and cobalt porphyrin for catalytic oxygen reduction in alkaline and acidic electrolytes

Rongzhong Jiang*, Deryn Chu

Sensors and Electron Devices Directorate, U.S. Army Research Laboratory, 2800 Powder Mill Road, Adelphi, MD 20783-1197, USA

HIGHLIGHTS

- Highly active $CoFeN_x/C$ catalysts were obtained by the pyrolysis of hemin.
- ORR catalytic kinetics was analyzed in both alkaline and acidic electrolytes.
- The kinetic rate of ORR in alkaline was 4-times higher than in acidic electrolyte.
- Catalytic stability of ORR was enhanced by adding cobalt to heat-treated hemin.
- The order of the single fuel cell performances was acidic > neural > alkaline.

ARTICLE INFO

Article history:
Received 1 April 2013
Received in revised form
3 June 2013
Accepted 22 June 2013
Available online 4 July 2013

Keywords:
Oxygen reduction
Catalytic kinetics
Heat-treatment
Nitrogen doped carbon
Alkaline membrane fuel cell

ABSTRACT

Comparative studies of the oxygen reduction kinetics and mechanisms of $CoFeN_x/C$ catalysts have been conducted with rotating disk electrode (RDE) and rotating ring-disk electrode (RRDE) in aqueous acid and alkaline solutions, as well as acidic and alkaline polymer electrolytes. The $CoFeN_x/C$ catalysts in this study were obtained by the pyrolysis of hemin and a cobalt porphyrin. In an alkaline electrolyte, a larger electron transfer coefficient (0.63) was obtained in comparison to that in an acidic electrolyte (0.44), signifying a lower free energy barrier for oxygen reduction. The kinetic rate constant (2.69×10^{-2} cm s^{-1}) for catalytic oxygen reduction in alkaline solution at 0.6 V (versus RHE) is almost 4 times larger than that in acidic solution (7.3×10^{-3} cm s^{-1}). A synergetic catalytic mechanism is proposed. The overall reduction is a 4-electron reduction of oxygen. The obtained $CoFeN_x/C$ catalyst was further evaluated as a cathode catalyst in single fuel cells with acidic, neutral and alkaline electrolyte membranes. The order of the single cell performances either for power density or for stability is acidic > neutral > alkaline. The different behaviors of the $CoFeN_x/C$ catalyst in half cell and single cell are discussed.

Published by Elsevier B.V.

1. Introduction

Intense research and development of fuel cells have been being carried out since 1990s. It is a promising technology to directly convert the chemical energy of fuel to electricity for transportation and consumer electronics. The proton exchange membrane fuel cell (PEMFC) has been targeted for producing commercial fuel cell vehicles. A number of prototype and demonstration cars based on PEMFCs have been released since 2009. Unfortunately, these prototype fuel cell cars made with PEMFC cost more than one million dollars. One of the biggest obstacles for PEMFCs is expensive electrode catalysts that are made from platinum based or other noble metals. To solve the cost issue of fuel cell catalysts, the alkaline electrolyte membrane fuel cell (AEMFC) has been proposed [1–5]. In an alkaline electrolyte, a fuel cell is able to use low cost non-noble metal catalysts. Non-noble metal catalysts, such as nickel based catalysts, have demonstrated much higher stability and better kinetic rates in alkaline electrolytes than in acidic electrolytes [6–9]. Heat-treated organic macrocyclic compounds containing nitrogen atoms have also demonstrated high catalytic activity for oxygen reduction reaction (ORR). A number of heat-treated macrocycles based on metalloporphyrins and phthalocyanines [10–17] have been reported with catalytic activity near that to noble metal platinum for ORR. Later people discovered that

* Corresponding author. Tel.: +1 301 394 0295; fax: +1 301 394 0273.
E-mail address: Rongzhong.jiang.civ@mail.mil (R. Jiang).

0378-7753/$ – see front matter Published by Elsevier B.V.
http://dx.doi.org/10.1016/j.jpowsour.2013.06.123

similar ORR catalysts can be obtained by the heat-treatment of various other nitrogen containing compounds; and the resulting catalysts (e.g., FeN_x/C or CoN_x/C) are called nitrogen doped carbon materials [18–26]. Further, it has been reported that heat-treated porphyrins containing Fe and Co atoms show better catalytic activity and stability than a heat-treated porphyrin containing only a single metal atom [13,18,24]. In these previous reports, an ORR catalyst was studied separately, either in acidic electrolyte or in alkaline electrolyte. For the same ORR catalyst, there is lack of comparative data between alkaline and acidic electrolytes. In the present article we perform a comparative study of $CoFeN_x/C$ catalyst, obtained by pyrolysis of hemin and cobalt tetrakis (methoxyphenyl) porphine (CoTMPP), for oxygen reduction in alkaline and acidic electrolytes. Previously, Gang Wu et al. [21] have studied carbon based CoFe binary non-precious metal catalysts for oxygen reduction with half and single fuel cell, respectively. They concluded that the optimal binary CoFe-based catalyst exhibits an improved activity and durability for oxygen reduction when compared to Fe- and Co-alone catalysts. Therefore, the second goal of the present article is to compare operational performance between half cell and single fuel cell. For single fuel cell research, we will use acidic, neutral, and alkaline electrolyte membranes to fabricate the membrane electrode assembly (MEA), and use the $CoFeN_x/C$ as cathode catalyst.

2. Experimental

2.1. Materials synthesis and processing

Carbon black (XC72R) was provided as a gift by Cabot®. Hemin from porcine and 5,10,15,20-tetrakis(4-methoxyphenyl)-21*H*,23*H*-porphine cobalt(II) (CoTMPP) were purchased from Aldrich. In a typical synthesis hemin, CoTMPP and XC72R were mixed in 0.5:0.5:1.0 weight ratio with an *N*,*N*-dimethylformamide (**DMF**) solvent. The mixture was stirred for half an hour at 100 °C. After stirring, the solvent was removed by evaporation. The remaining dry mixture was heat-treated in a tubular furnace under a N_2 atmosphere at 700 °C for 2 h. The furnace was then cooled to 40 °C. The final product was collected. The heat-treated mixture was processed with ultrasonic treatment. A Branson Sonifier 450 Analog Ultrasonic Homogenizer 1/2″ diameter disrupter horn was used for this process. After 2–3 h of the ultrasonic processing while being cooled with ice, the sample was removed and dried in an oven at 80 °C. The catalyst sample produced after the heat-treatment and ultrasonic processing steps is expressed as $CoFeN_x/C$.

2.2. Electrochemical analysis of half cell

A Pine Bipotentiostat RDE4 was used for electrochemical analysis of the half cell containing the synthesized catalysts. First, 100 mg of the $CoFeN_x/C$ catalyst sample was processed into an ink by adding 2 mL water, 2 mL ethanol and 500 mg of a 5 wt% Nafion solution (or 25 mg net Nafion). A uniform ink was obtained by ultrasonic treatment with a Branson 3510 ultrasonic bath at 100 W and 40 KHz. Next, 10 μl of catalyst ink was coated onto a glassy carbon (**GC**) disk as a working electrode (0.247 cm^2), and dried at 30 °C under vacuum for 3 h. The catalyst loading was approximately 1 mg cm^{-2} $CoFeN_x/C$. The catalyst coated electrode was mounted onto a Pine ASR rotator. Rotating disk electrode (RDE) experiments were performed in O_2 or argon saturated electrolyte solutions at room temperature (20 ± 1 °C). The electrolyte solutions were 0.5 M H_2SO_4 and 0.1 M KOH, respectively. A platinum wire counter electrode and a saturated calomel reference electrode (SCE) were used for all studies. The SCE was converted to the reversible hydrogen electrode (RHE) for this report. A rotating ring disk electrode (RRDE) was used to detect H_2O_2 during the oxygen reduction experiment. The RRDE had a measured collection efficiency of 0.37. A ring potential of 1.4 V (versus RHE) was applied to make sure the collected H_2O_2 was completely oxidized to water on the ring electrode. The current density reported in this article is based on the geometrical disk area of the electrode (mA cm^{-2}).

2.3. Electrochemical analysis of a single fuel cell

For single fuel cell experiments, the synthesized $CoFeN_x/C$ was used as the cathode catalyst. Three types of polymer electrolyte membranes, H^+ type, K^+ type and OH^- type, were used. The cathode catalyst ink was prepared with 80% catalyst material and 20% binder. Total cathode catalyst material loading of $CoFeN_x/C$ on the electrode was 2.5 mg cm^{-2}. Johnson Matthey's 40% carbon supported Pt black was used to prepare anode catalyst ink with 80% catalyst (carbon plus Pt) and 20% binder. Pt loading on the anode electrode was 0.4 mg cm^{-2}. The cathode and anode catalyst inks were coated on two pieces of 5 cm^2 and 0.3 mm thick water proof carbon papers (TGP-H-090), respectively. The polymer electrolyte membranes for this research were H^+ type Nafion 211, K^+ type Nafion 211, and A201 alkaline membrane. The H^+ type of Nafion 211 was purchased from Du Pont. The K^+ type of Nafion 211 was obtained by neutralization of the H^+ type of Nafion 211 with KOH. The A201 alkaline membrane was purchased from Tokuyama Company. The binders for acidic, neutral, and alkaline fuel cells were solution type of Nafion, KOH neutralized Nafion, and Tokuyama AS-4 ionomers, respectively. Three corresponding types of MEAs were prepared by hot pressing the cathode, polymer electrolyte membrane, and anode together. The pressing temperature was 120 °C for the Nafion membranes and 40 °C for the A201 alkaline membrane. A single cell was fabricated by simply placing a freshly prepared MEA into a commercially available single cell test device (purchased from Fuel Cell Technology, Inc.) that consisted of two graphite plates. There were two sets of micro channels for fuel and oxidant flows, respectively, on the interior sides of the graphite plates. On the exterior sides of the graphite plate, there were two copper plates for inserting two heaters and a thermal couple. There were also four electric leads to collect current and voltage from the fuel cell and send current and voltage to a fuel cell test instrument. These single cell setups were tested with a Fuel Cell Test Station purchased from Fuel Cell Technology, Inc. Both fuel and oxidant were humidified and preheated automatically by passing through the Fuel Cell Test Station before entering the fuel flow channel. In the single cell experiment, we used O_2 as oxidant and H_2 as fuel, with flow rates 200 and 100 sccm, respectively.

3. Results and discussion

3.1. Half cell results

3.1.1. Surface waves of $CoFeN_x/C$ coated GC electrode in acidic and alkaline electrolytes

Fig. 1 shows cyclic voltammograms of $CoFeN_x/C$ coated GC electrode in argon saturated acidic and alkaline electrolytes, respectively. In 0.5 M H_2SO_4 solution, a couple of symmetric peaks are clearly seen. The average peak potential of the anodic and the cathodic peaks is about 0.62 V. With increasing scan rate, the peak current increases. The plot of peak current versus scan rate is a straight line, and the peak current is proportional to scan rate. This electrode reaction appears to be independent of diffusion. This could represent surface waves of the oxidation of active sites and subsequent reduction at the $CoFeN_x/C$ GC electrode in acidic electrolyte. The catalytic activity is relative to the transition metals doped in the carbon materials. The transition metal plays the role of

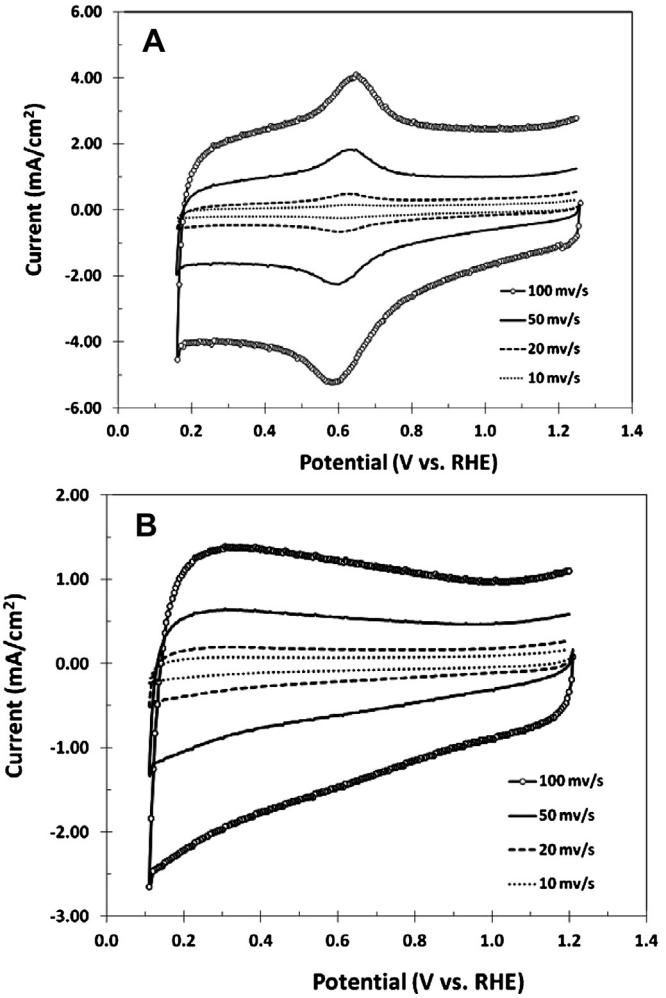

Fig. 1. Cyclic voltammograms for a $CoFeN_x$/C catalyst coated GC electrode in argon saturated 0.5 M H_2SO_4 (A) and 0.1 M KOH electrolytes (B).

a mediator in the electron transfer process occurring between the oxygen molecules and the metal ions, and between the metal ions and the electrode. During this process, there must be a valence changes between Fe(II) and Fe(III). Unexpectedly, by switching from a 0.5 M H_2SO_4 electrolyte to a 0.1 M KOH electrolyte, such symmetric waves do not appear for the same experiment. In Fig. 1B, the voltammograms exhibit only charging current in argon saturated 0.1 M KOH solution for scan rate varying from 10 mv s^{-1} to 100mv s^{-1}. The absence of the surface waves at the $CoFeN_x$/C coated GC electrode is not clearly understood. It is probably because no electrochemical oxidation/reduction occurs, or no valence change at the active metal sites for the heat-treated catalyst in alkaline solution. Similar phenomenon of disappearing surface oxidation/reduction waves were reported for heat-treated Fe(III) tetramethoxyphenyl porphyrin supported on active carbon in alkaline solution by R. F. Savinell et al. [27]. In their report, the symmetric wave disappearance was found to be dependent on heat-treatment temperature. Such symmetric waves were only seen for alkaline solutions when the heat-treatment temperature was less than 200 °C. If heat treatment was higher than 400 °C, the metalloporphyrin's chemical structure changed, causing the catalyst coated electrode being non-active in argon saturated alkaline electrolyte while remaining active in acidic electrolyte.

3.1.2. Effect of acidic and alkaline electrolytes on the catalytic activity of ORR

When oxygen gas is passing through the electrolyte solutions, the $CoFeN_x$/C coated GC electrode shows high catalytic activity for oxygen reduction in both acidic and alkaline electrolytes. However, because it has a more positive catalytic peak potential and higher catalytic current, the catalytic activity for oxygen reduction is higher in alkaline electrolyte than that in acidic electrolyte. Fig. 2 shows cyclic voltammograms of $CoFeN_x$/C coated GC electrode in O_2 saturated 0.5 M H_2SO_4 and 0.1 M KOH solutions, respectively. The catalytic peak corresponding to O_2 reduction appears at 0.75 V for 0.5 M H_2SO_4, and 0.85 V for 0.1 M KOH, respectively. Comparing the cyclic voltammograms in Figs. 1 and 2 for O_2 and argon saturated 0.5 M H_2SO_4 solution, we find that the cathodic peak potential is slightly higher in O_2 saturated solution than that in argon saturated solution (0.75 V versus 0.62 V). This is typical of a catalytic wave in O_2 saturated acidic solution, which involves valence changes on the active catalytic sites at the $CoFeN_x$/C catalyst and fast electron transfer between the active metal centers and the electrode. Although the $CoFeN_x$/C coated GC electrode shows no symmetric surface waves in argon saturated alkaline solution, it gives even higher catalytic activity for oxygen reduction in alkaline solution than that in acidic electrolyte. From the results in Figs. 1 and 2, we know there may be different catalytic mechanisms for oxygen reduction in acidic and alkaline electrolytes. The kinetics of oxygen reduction in acidic and alkaline electrolytes will be analyzed in the following, in order to understand the mechanisms for oxygen reduction.

3.1.3. Catalytic analysis of ORR kinetics in acidic and alkaline electrolytes

The mechanisms of oxygen reduction at $CoFeN_x$/C coated GC electrode can be better understood by analysis of the catalytic kinetics. Fig. 3 shows polarization curves of $CoFeN_x$/C coated rotating GC disk electrode in O_2 saturated 0.5 M H_2SO_4 and O_2 saturated 0.1 M KOH solutions, respectively. With increasing rotation rate, the polarization curve of 0.5 M H_2SO_4 does not reach limiting current and does not exhibit a flat plateau; but, the polarization curve for 0.1 M KOH shows flat plateaus for all rotation rates. The kinetic parameters of both conditions can be obtained by Tafel plots.

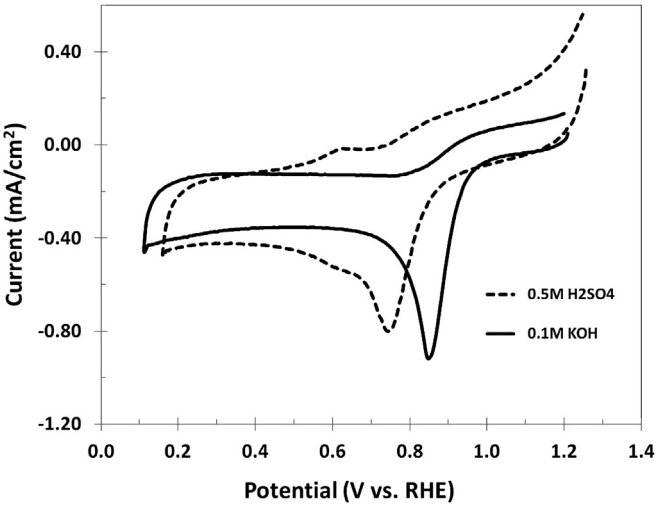

Fig. 2. Cyclic voltammograms for a $CoFeN_x$/C catalyst coated GC electrode in O_2 saturated 0.5 M H_2SO_4 (dashed line) and 0.1 M KOH electrolytes (solid line).

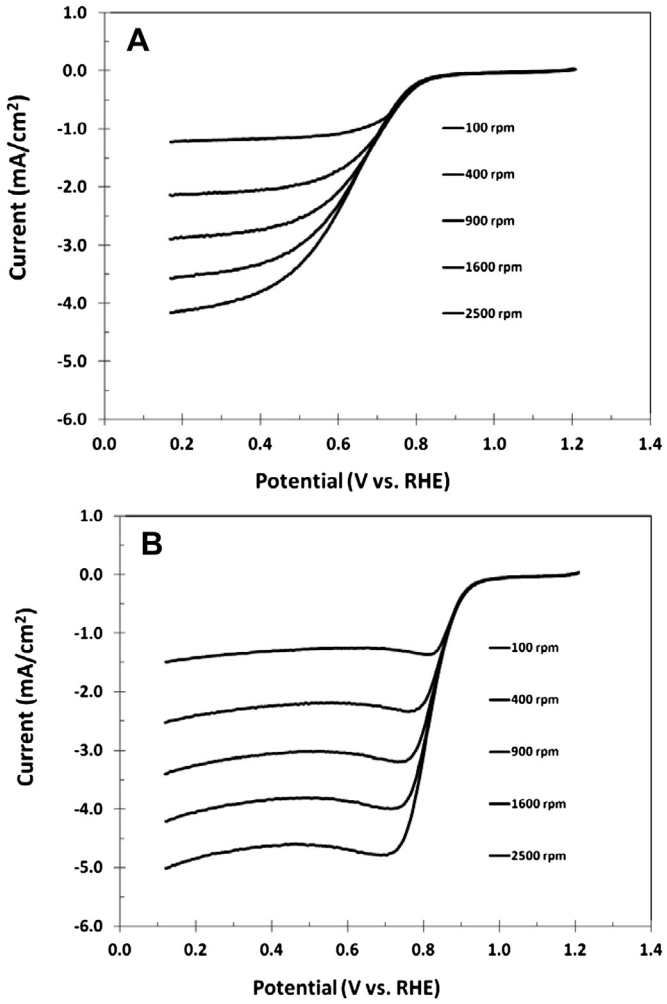

Fig. 3. Polarization curves for a $CoFeN_x$/C catalyst coated rotating GC disk electrode in O_2 saturated 0.5 M H_2SO_4 (A) and 0.1 M KOH electrolytes (B).

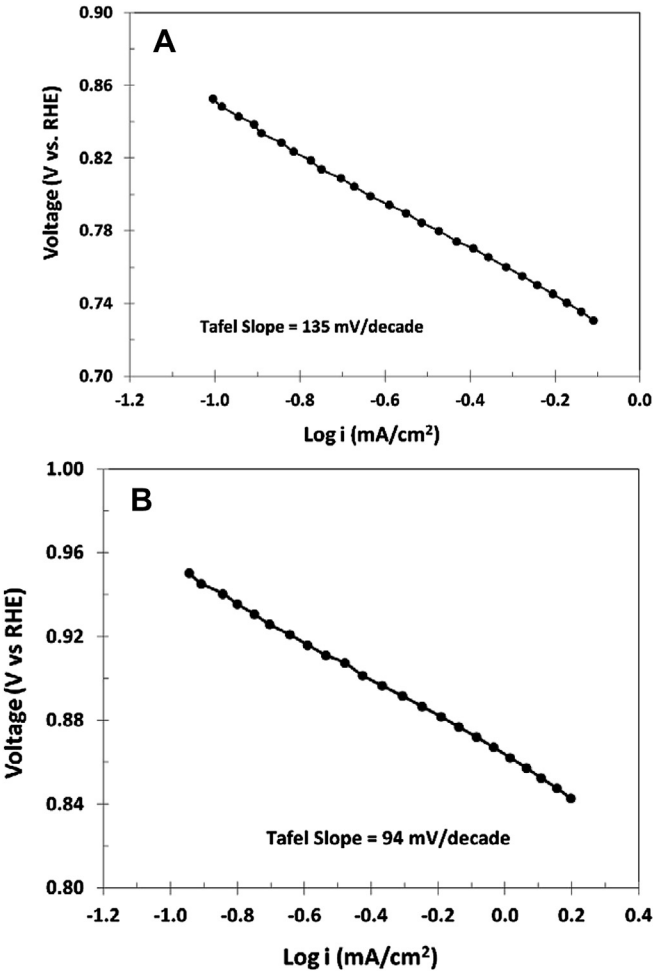

Fig. 4. Tafel plots of the polarization curves for a $CoFeN_x$/C catalyst coated rotating GC disk electrode in O_2 saturated 0.5 M H_2SO_4 (A) and 0.1 M KOH electrolytes (B).

$$E = E^0 + \frac{2.303RT}{\alpha n_\alpha F}\mathrm{Log}\left(i^0\right) - \frac{2.303RT}{\alpha n_\alpha F}\mathrm{Log}(i) \quad (1)$$

$$i^0 = nFK_eC_o \quad (2)$$

Here, E and E^0 are experimental disk potential and thermodynamic electrode potential under the experimental conditions ($E^0 = 1.23$ V vs. RHE), respectively; α is the electron transfer coefficient in the rate-determining step for oxygen reduction; n_α is the electron transfer number at the rate determining step; i^0 is the exchange current density, or the current density at the absence of net electrochemical reactions and at zero overpotential; i is the disk current; K_e is the electron transfer rate constant in rate determining step; C_o is oxygen concentration at the electrode surface (for low current density and O_2 saturated electrolyte, $C_o \approx 1.3 \times 10^{-6}$ mol cm^{-3}) [32]; n is the electron number of overall oxygen reduction; and, the R, T, and F have their common meanings of universal gas constant (8.314 J mol^{-1} K^{-1}), absolute temperature (K), and Faraday's constant (96,485 C mol^{-1}), respectively.

The pure kinetic current appears at the low current density region of the polarization curves. This is the beginning portion of the polarization curves for oxygen reduction, where the current does not change with increasing rotation rate. Fig. 4 shows Tafel plots (E versus log i) of the polarization curves of $CoFeN_x$/C catalyst coated rotating GC disk electrode in O_2 saturated 0.5 M H_2SO_4 and 0.1 M KOH electrolytes, respectively. From the Tafel slope, the α value can be obtained by considering n_α as 1 (the electron number at the rate determining step is 1). The i^0 and k_e can be then calculated from the intercept. These kinetic parameters are listed in Table 1. In 0.1 M KOH solution, a smaller Tafel slope (94 mv dec^{-1}) is obtained, resulting in larger α value (0.629). The larger α value signifies larger fraction of the interfacial potential at the electrode–KOH electrolyte interface, which helps in lowering free energy barrier for oxygen reduction in 0.1 M KOH solution. It is interesting that the kinetic parameters of i^0 and K_e are very close for the catalysts in 0.5 M H_2SO_4 and 0.1 M KOH. L. Zhang et al. [22] reported that the parameters of i^0 and K_e of oxygen reduction in 0.5 M H_2SO_4 vary with catalytic site concentration for Fe–N/C type of catalysts. With increasing Fe concentration, the values of i^0 and K_e increase. If the coverage of catalyst layer is too high, the values of i^0 and K_e should

Table 1
Comparison of kinetic parameters of the rate determining step of oxygen reduction in 0.5 M H_2SO_4 and 0.1 M KOH.

Electrolyte	α	i^0 (A cm^{-2})	K_e (cm s^{-1})	Tafel slope (mV dec^{-1})	Intercept (V)
0.5 M H_2SO_4	0.438	1.55×10^{-7}	3.29×10^{-7}	135	0.716
0.1 M KOH	0.629	1.28×10^{-7}	2.91×10^{-7}	94	0.864

decrease with increasing Fe concentration. There is no report on comparison of i^0 and K_e between acidic and alkaline electrolytes. It seems that changing electrolyte pH will affect the α value, but not the parameters of i^0 and K_e as the concentration of catalyst sites is unchanged because the same catalyst is used in the acidic and alkaline electrolytes. The slightly smaller kinetic data of i^0 and K_e listed in Table 1 than those reported by L. Zhang [22,23] are attributed to a lower concentration of catalytic sites.

Further kinetic analysis of catalytic oxygen reduction at the high current density part can be carried out by Levich plot and Koutcky–Levich plot of the polarization curves in Fig. 3.

$$i_L = 0.620nFAD_o^{2/3}\omega^{1/2}\nu^{-1/6}C_o^* \quad (3)$$

$$i_k = nFAK_f(E)C_o^* \quad (4)$$

$$i^{-1} = i_k^{-1} + i_L^{-1} \quad (5)$$

$$i^{-1} = \frac{1}{nFAK_f(E)C_o^*} + \frac{1}{0.620nFAD_o^{2/3}\nu^{-1/6}C_o^*\omega^{1/2}} \quad (6)$$

Here, i_L is Levich current for species O's electrode reaction by diffusion controlled process; A is the electrode area (cm^2); D_o ($cm^2\ s^{-1}$) is diffusion coefficient of Species O; ω (s^{-1}) is rotation rate ($=2\pi f = 2\pi \times$ rpm/60); ν ($cm^2\ s^{-1}$) is viscosity of electrolyte solution; C_o^* is oxygen concentration in bulk electrolyte solution (in O_2 saturated electrolyte, $C_o^* = 1.3 \times 10^{-6}$ mol cm^{-3}) [31]; i_k is kinetic current of O species at the electrode surface; and $K_f(E)$ ($cm\ s^{-1}$) is rate constant of oxygen reduction at potential E.

The Koutecky–Levich plot, or the i^{-1} versus $\omega^{-1/2}$ plot from Eq. (6), should provide a straight line. We can obtain a kinetic rate constant for the oxygen reduction from the intercept, and the number of electrons transferred in the electrochemical reaction from the slope. In this study, the diffusion coefficient of O_2 is $1.7 \times 10^{-5}\ cm^2\ s^{-1}$ [32,33].

Fig. 5 shows Levich plots (i versus $\omega^{-1/2}$) and Koutcky–Levich plots (i^{-1} versus $\omega^{-1/2}$) of the polarization curves in Fig. 3A using 0.5 M H_2SO_4 as the electrolyte. These Levich plots are smooth curves, which bend down with increasing electrode potential; implying lower kinetic rate for oxygen reduction at higher electrode potentials. The Koutcky–Levich plots obtained from experiments are straight lines, and are parallel to the calculated

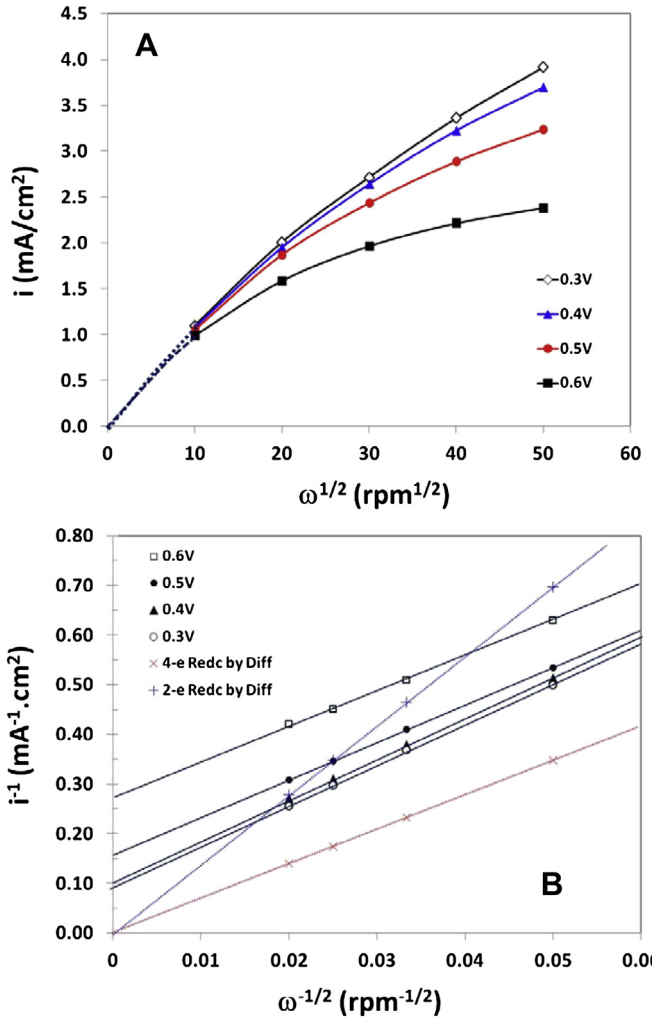

Fig. 5. Levich plots (A) and Koutcky–Levich plots (B) of the polarization curves for a $CoFeN_x$/C catalyst coated rotating GC disk electrode in O_2 saturated 0.5 M H_2SO_4. The dashed lines are calculated curves for 2-electron and 4-electron oxygen reduction by an O_2 diffusion controlled process, respectively.

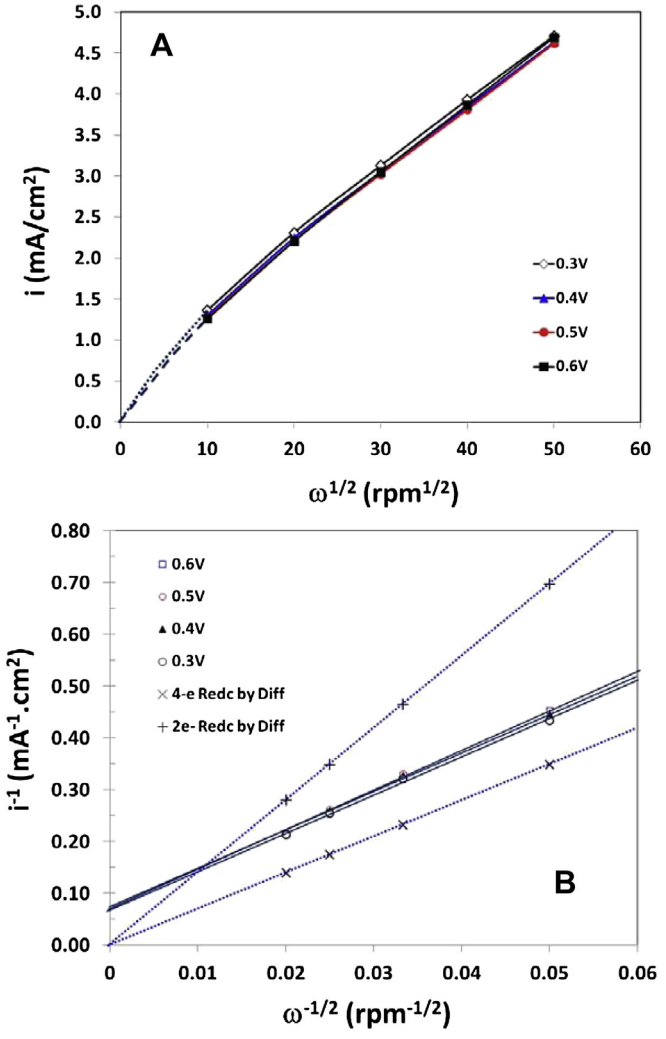

Fig. 6. Levich plots (A) and Koutcky–Levich plots (B) of the polarization curves for a $CoFeN_x$/C catalyst coated rotating GC disk electrode in O_2 saturated 0.1 M KOH. The dashed lines are calculated curves for 2-electron and 4-electron oxygen reduction by O_2 diffusion controlled process, respectively.

Table 2
Comparison of kinetic rates of catalytic oxygen reduction on a CoFeNx/C catalyst in 0.5 M H_2SO_4 and 0.1 M KOH.

Electrolyte	Kinetic rate, K_f, (cm s^{-1})			
	0.6 V	0.5 V	0.4 V	0.3 V
0.5M H_2SO_4	7.3×10^{-3}	1.25×10^{-2}	1.99×10^{-2}	2.21×10^{-2}
0.1M KOH	2.69×10^{-2}	2.76×10^{-2}	2.84×10^{-2}	2.93×10^{-2}

curve for 4-electron oxygen reduction by diffusion controlled process. This indicates that 4-electron oxygen reduction to water through H_2O_2 disproportion. Fig. 6 shows Levich plots and Koutcky–Levich plots of the polarization curves in Fig. 3B for using 0.1 M KOH as the electrolyte. In order to compare, we used the data in Fig. 6 having the same disk potentials with those in Fig. 5. From potentials 0.3 V to 0.6 V, the Levich plots in Fig. 6 are almost overlapped, which implies that the kinetic rates for oxygen reduction between 0.3 V and 0.6 V in 0.1 M KOH are less potential dependent, and reaching a limiting current. This claim is further supported by the Koutecky–Levich plots. The kinetic rates of the $CoFeN_x$/C coated GC electrode for catalytic oxygen reduction in 0.5 M H_2SO_4 and 0.1 M KOH are listed in Table 2. At 0.6 V the kinetic rate for oxygen reduction in 0.1 M KOH is about 4 times higher than that in 0.5 M H_2SO_4 solution. In alkaline solution, oxygen reduction has higher catalytic kinetic rate constants and larger electron transfer coefficients than in acidic electrolyte.

3.1.4. Rotating ring-disk electrode (RRDE) analysis

Further analysis of oxygen reduction and mechanisms at $CoFeN_x$/C can be obtained by rotating ring disk (RRDE) method. Fig. 7 shows polarization curves for a $CoFeN_x$/C catalyst coated rotating GC disk electrode and corresponding ring current at Pt-ring electrode in O_2 saturated 0.5 M H_2SO_4 (Fig. 7A) and 0.1 M KOH (Fig. 7C) electrolytes, respectively. Both conditions show a small ring current, indicating a small amount of hydrogen peroxide, which is produced in the oxygen reduction process. The electron number (n) for oxygen reduction can be calculated with the following equation,

$$n = \frac{4i_d}{i_d + i_r/N_r} \tag{7}$$

Here, i_d and i_r are experimental disk current and ring current, respectively. N_r is collection coefficient of the ring electrode.

Fig. 7B and D shows the calculated electron numbers of oxygen reduction at $CoFeN_x$/C coated GC electrode in 0.5 M H_2SO_4 and 0.1 M KOH, respectively. The average electron numbers of oxygen reduction are 3.8 for 0.5 M H_2SO_4, and 3.5 for 0.1 M KOH. These results indicate that a larger fraction of oxygen molecules are reduced through direct 4-electron reduction mechanism in acidic electrolyte than in alkaline electrolyte. This could also suggest that the oxygen molecules are adsorbed on the catalyst by a bridge model [24,29–31]. There is more possibility of oxygen reduction through hydrogen peroxide disproportional reaction [28] in alkaline solution.

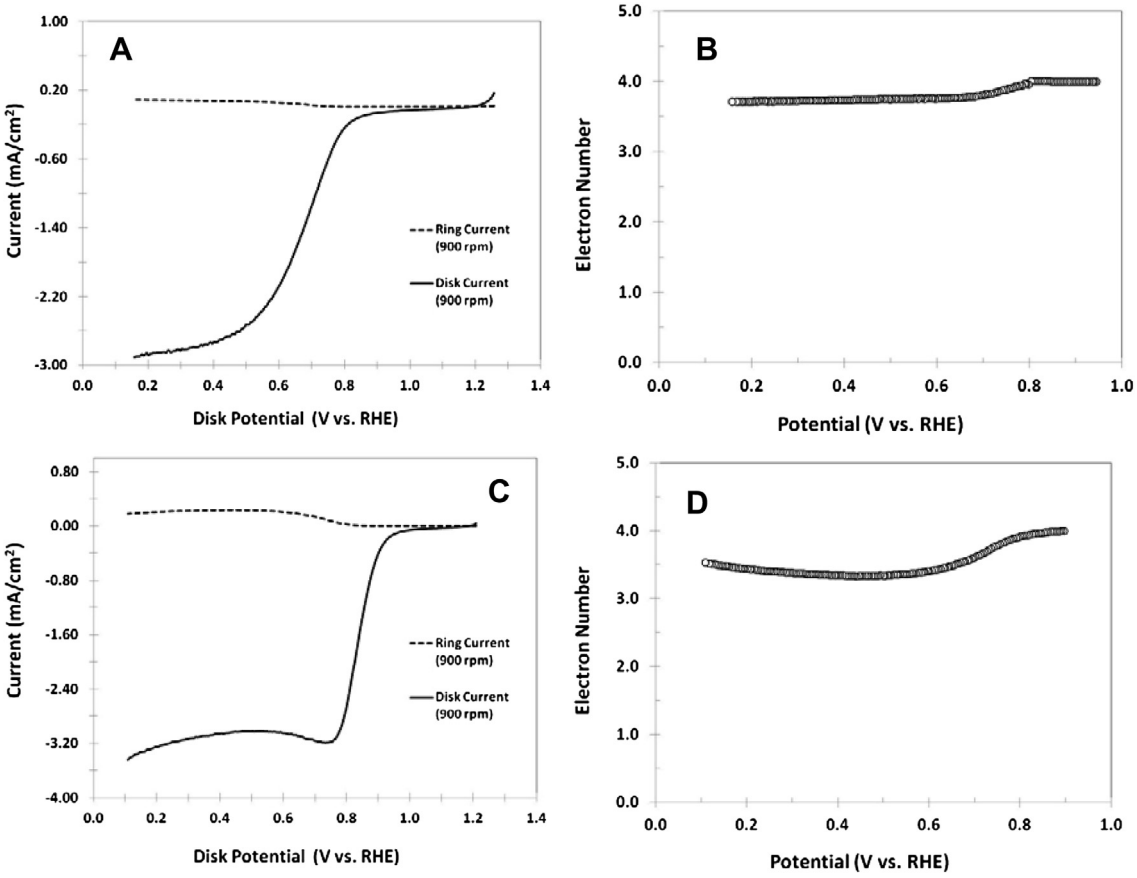

Fig. 7. RRDE polarization curves for a $CoFeN_x$/C catalyst coated rotating GC and Pt-ring electrodes in O_2 saturated 0.5 M H_2SO_4 (A) and 0.1 M KOH electrolytes (C); and calculated electron number for O_2 reduction in 0.5 M H_2SO_4 (B) and 0.1 M KOH (D) electrolytes, respectively.

3.1.5. Oxygen reduction mechanisms in acidic and alkaline electrolytes

Based on (i) systemic half cell experiments using the $CoFeN_x/C$ catalyst coated electrodes in argon and oxygen saturated acidic and alkaline electrolytes and (ii) kinetic analysis of catalytic oxygen reduction using RDE and RRDE experiments, the mechanisms of oxygen reduction in acidic and alkaline solutions may be discussed. Camacho and Stevenson et al. [28] have proposed an oxygen reduction mechanism for nitrogen doped (N-doped) carbon nanotubes containing transition metal ions. They indicated that oxygen reduction at the N-doped carbon surface occurs by the 2-electron reduction of oxygen to hydrogen peroxide, followed by disproportion on the transition metal Fe(II) ion to produce water and oxygen. The overall reaction is a 4-electron reduction. Here, we proposed a modified mechanism for the oxygen reduction at the catalyst obtained by the heat-treatment of hemin and a cobalt porphyrin supported on carbon black. Separate mechanisms are proposed for the catalysts in both acidic and alkaline electrolytes.

In an acidic electrolyte, the proposed oxygen reduction mechanism is:

$$PM^{3+} + e^- \leftrightarrow PM^{2+} \tag{8}$$

$$PM^{2+} + O_2 \rightarrow \left(PM^{3+}\cdots\cdots O_2^-\right)_{ads} \tag{9}$$

$$\left(PM^{3+}\cdots\cdots O_2^-\right)_{ads} + e^- + 2H^+ \rightarrow PM^{3+} + H_2O_2 \tag{10}$$

$$2H_2O_2 + PM^{3+} \rightarrow O_2 + 2H_2O + PM^{3+} \tag{11}$$

Here, PM expresses the heat-treated catalyst containing transition metals Co and Fe. In the catalytic process, the metal centers have valence changes between M^{3+} and M^{2+}. The $(PM^{3+}\cdots\cdots O_2^-)_{ads}$ expresses an adsorption complex of the catalyst site with an oxygen molecule. The oxygen molecules are catalytically reduced to water through a step yielding an H_2O_2 intermediate and the subsequent disproportional reaction of the intermediate product.

In alkaline electrolyte, the oxygen reduction mechanism is slightly different:

$$PM^{2/3+} + O_2 \leftrightarrow \left(PM^{2/3+}O_2\right)_{ads} \tag{12}$$

$$\left(PM^{2/3+}O_2\right)_{ads} + e^- \rightarrow \left(PM^{2/3+}O_2^{\bullet-}\right)_{ads} \tag{13}$$

$$\left(PM^{2/3+}O_2^{\bullet-}\right)_{ads} + e^- + H_2O \rightarrow \left(PM^{2/3+}O_2^{2-}\cdots\cdots H_2O\right)_{ads} \tag{14}$$

$$\left(PM^{2/3+}O_2^{2-}\cdots\cdots H_2O\right)_{ads} \rightarrow HO_2^- + OH^- + PM^{2/3+} \tag{15}$$

In alkaline solution, there are no valence changes recognized on the cyclic voltammogram of $CoFeN_x/C$ coated GC electrode in argon saturated 0.1 M KOH solution. Here, we use of $PM^{2/3+}$ to express the catalyst site, due to the uncertainty of the valence state of the Fe and Co. The $(PM^{2/3+}O_2^{\bullet-})_{ads}$ is an adsorption complex of the oxygen radical species on the catalyst site, or an intermediate product of oxygen reduction.

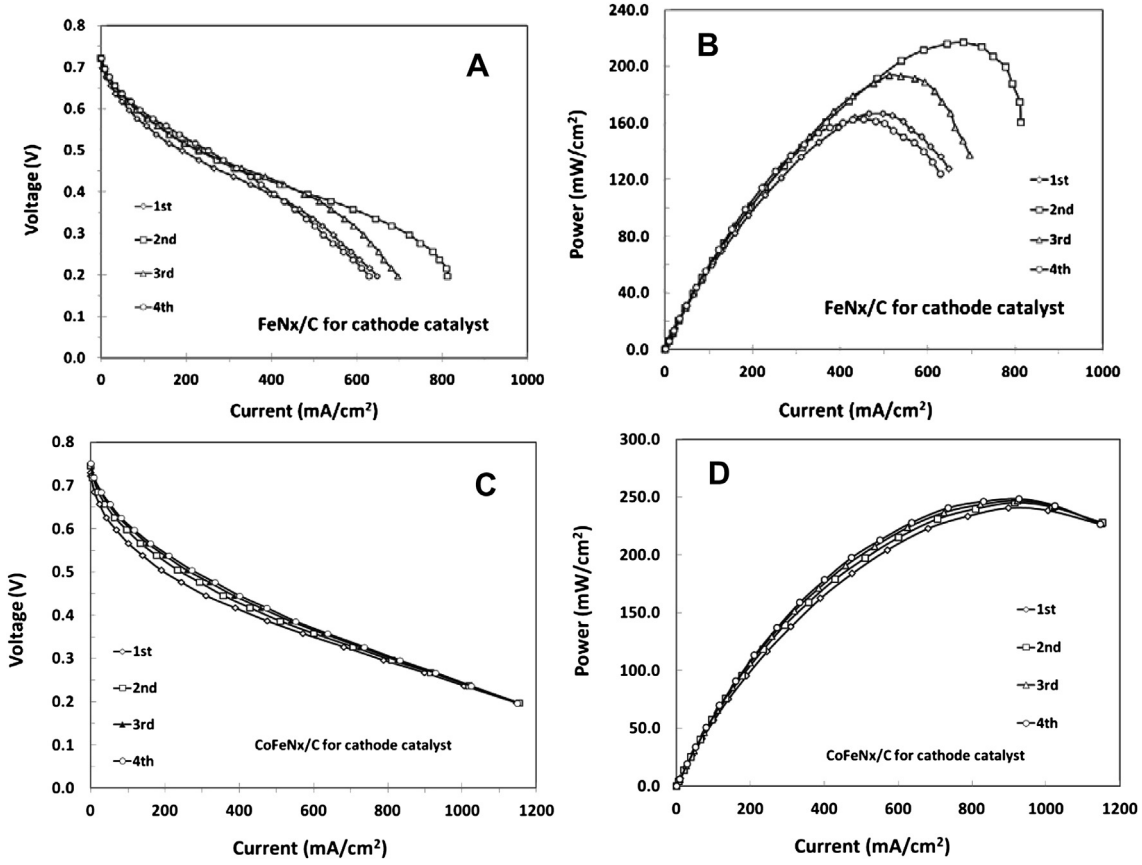

Fig. 8. Single fuel cell performance measured using a single metal catalyst (FeN_x/C) and a bi-metal catalyst ($CoFeN_x/C$) as the cathode catalyst. A and B, voltage–current (A) and power current (B) curves of a single H_2/O_2 fuel cell using FeN_x/C as the cathode catalyst; C and D, voltage–current (C) and power current (D) curves of a single H_2/O_2 fuel cell using $CoFeN_x/C$ as the cathode catalyst. The anode catalysts were 40% Pt/C for both cells. Nafion 211 was used as the electrolyte membrane. Operating temperature for all experiments was 60 °C.

In addition to the mechanism of oxygen reduction through the formation of an H_2O_2 intermediate, there is also a probability for oxygen reduction through direct 4-electron reduction to water. The direct 4-electron oxygen reduction process requires that the oxygen is adsorbed simultaneously by two metal sites (i.e., a bridge adsorption) [24,29–31].

3.2. Single fuel cell results

3.2.1. Synergetic effect of Co/Fe binary transition metals on cell performance

Results from a half cell using FeN_x/C for catalytic oxygen reduction have been reported in literature [15]. These reports demonstrate very good catalytic activity for the 4-electron reduction of oxygen to water; however, these reports do not examine the catalytic stability of the material. Therefore, in order to compare it with the $CoFeN_x/C$ catalyst, we report the single cell results of FeN_x/C in this article. For practical applications, an electrode catalyst must be evaluated in a single fuel cell. First, we should explain why we opt for the use of a $CoFeN_x/C$ catalyst containing mixed cobalt and iron metal sites instead of single metal sites. The single metal CoN_x/C catalyst has good stability for oxygen reduction, but favors the catalysis of oxygen in a 2-electron reduction to hydrogen peroxide [13,31,34]. The single metal FeN_x/C catalyst favors the catalysis of oxygen in a 4-electron reduction to water, but has poor stability [11,13,15]. The combination of these two single metal

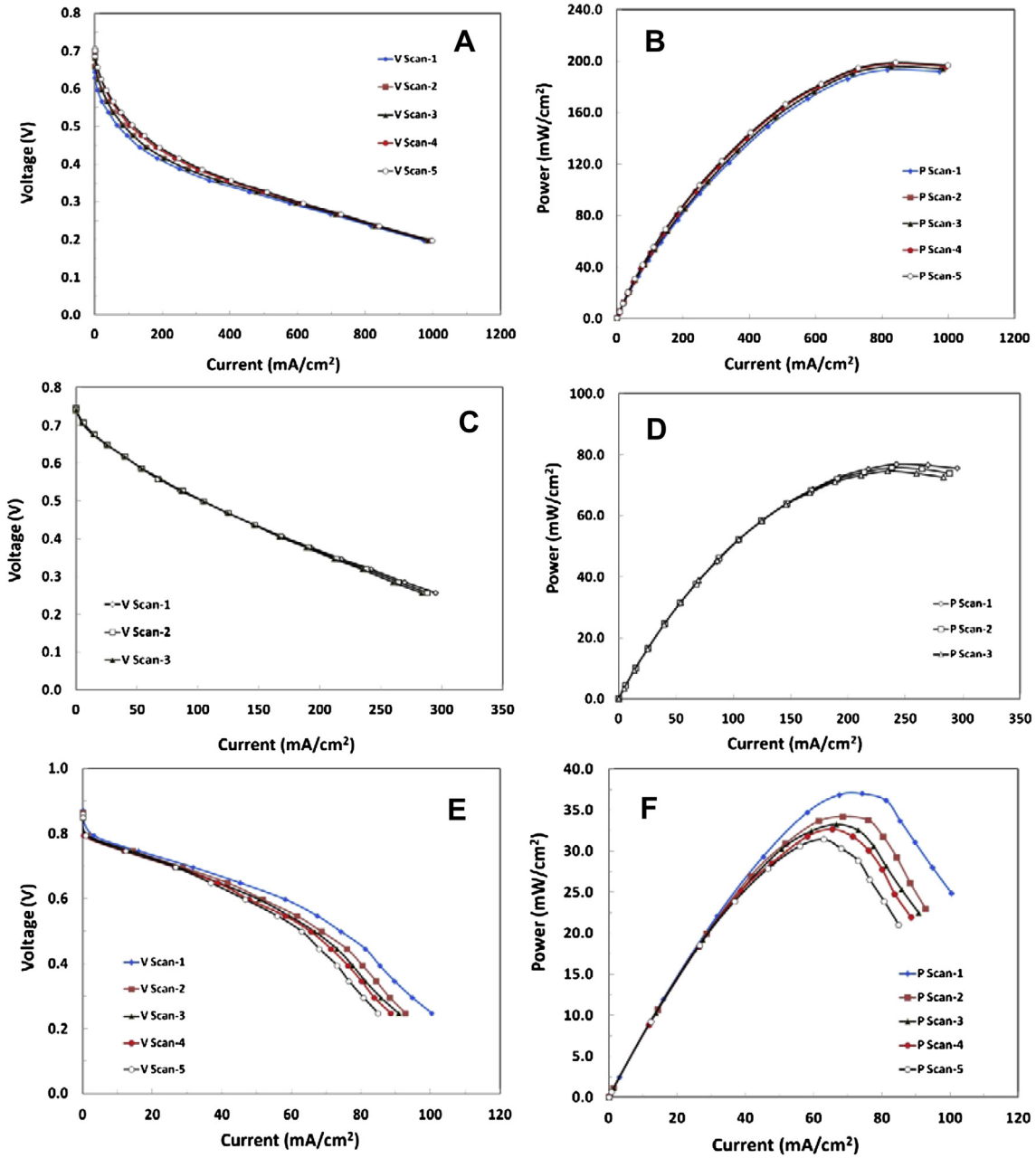

Fig. 9. Effect of acid, neutral, and alkaline membranes on the single cell performance with a fuel cell using $CoFeN_x/C$ as the cathode catalysts and 40% Pt/C as the anode catalysts. A and B, H^+-type Nafion 211 was used as the electrolyte membrane; C and D, K^+-type Nafion 211 was used as the electrolyte membrane; and E and F, Tokuyama A201 (alkaline) was used for the electrolyte membrane (KOH free). Operating temperature for all experiments was 40 °C.

catalysts may have a synergetic effect for realizing both good stability and a 4-electron reduction of oxygen to water. Fig. 8 shows the single fuel cell performances using Nafion 211 as electrolyte membrane with single metal catalyst FeN_x/C and bi-metal catalyst $CoFeN_x/C$ as the cathode catalysts, respectively. The fuel cell using FeN_x/C as the cathode catalyst (Fig. 8A and B) shows good initial catalytic activity on the first scan; however, the power density continuously drops with subsequent scans. Apparently, the single metal FeN_x/C catalyst is not sufficiently stable for a practical fuel cell. When the single metal FeN_x/C catalyst is replaced by a bi-metal $CoFeN_x/C$ catalyst, the fuel cell gives higher catalytic current density and larger peak power density (Fig. 8C and D). The fuel cell performance slightly increases with consecutive scans, until stable current and power values are reached (see the top curves in Fig. 8C and D). The improved single fuel cell performance at $CoFeN_x/C$ catalyst is attributed to the synergetic effect of the bi-metal catalysts. The hydrogen peroxide produced by the catalysis of CoN_x/C is further reduced to water at the FeN_x/C catalyst.

3.2.2. Single fuel cell performance with acidic, neutral and alkaline membranes

The good half cell performance of the $CoFeN_x/C$ catalyst, demonstrated with RDE and RRDE experiments, encouraged us to carry out single fuel cell experiments with acidic, neutral, and alkaline electrolyte membranes. These single cell results with the $CoFeN_x/C$ catalyst and different electrolyte membranes are summarized in Fig. 9. Here, we used $CoFeN_x/C$ as the cathode catalysts for all these single fuel cells. The H^+-type Nafion 211, K^+-type Nafion 211, and Tokuyama A201 are used as the acidic, neutral and alkaline electrolyte membranes, respectively. Surprisingly, the order of the single fuel cell performances is acidic > neutral > alkaline, for both activity and stability. When H^+-type Nafion 211 is used as the electrolyte membrane, the fuel cell performance is stable, having peak power density 200 mW cm^{-2}. The single fuel cell using the K^+-type Nafion 211 as the electrolyte membrane is still stable and demonstrates a peak power density 77 mW cm^{-2}. However, when the Tokuyama A201 is used as the electrolyte membrane, the polarization current is unstable, and decreases with consecutive scans. The peak power density for the first scan with Tokuyama 201 electrolyte membrane is only 37 mW cm^{-2}; about 1/3 magnitude of the peak power density by using H^+-type Nafion 211 as electrolyte membrane. To understand the phenomenon of opposite order of single cell performance versus the half cell performance with acidic and alkaline electrolytes, we further examined the stability of Tokuyama A201 electrolyte membrane using 40% Pt black to replace the $CoFeN_x/C$ catalyst as the cathode catalyst. There were no other changes in the fuel cell conditions. Fig. 10 shows voltage–current and power–current curves of a single H_2/O_2 fuel cell using 40% Pt/C as both cathode and anode catalysts, Tokuyama A201 (alkaline) as electrolyte membrane (KOH free), and a 60 °C cell temperature. It is already known that 40% Pt/C black is a stable cathode catalyst for H_2/O_2 fuel cell with acidic electrolyte membrane (i.e., Nafion). Unfortunately, the single fuel cell using 40% Pt/C as cathode catalyst with the Tokuyama A201 alkaline electrolyte membrane is still not stable, as shown in Fig. 10A and B. With consecutive scans, both the current density and the power density decrease continuously. The experimental results in Fig. 9 further demonstrate that the present alkaline electrolyte membranes are not sufficient for alkaline fuel cell in free KOH operating conditions. Our experimental results indicate that the development of a suitable alkaline electrolyte membrane is essential for alkaline membrane fuel cell.

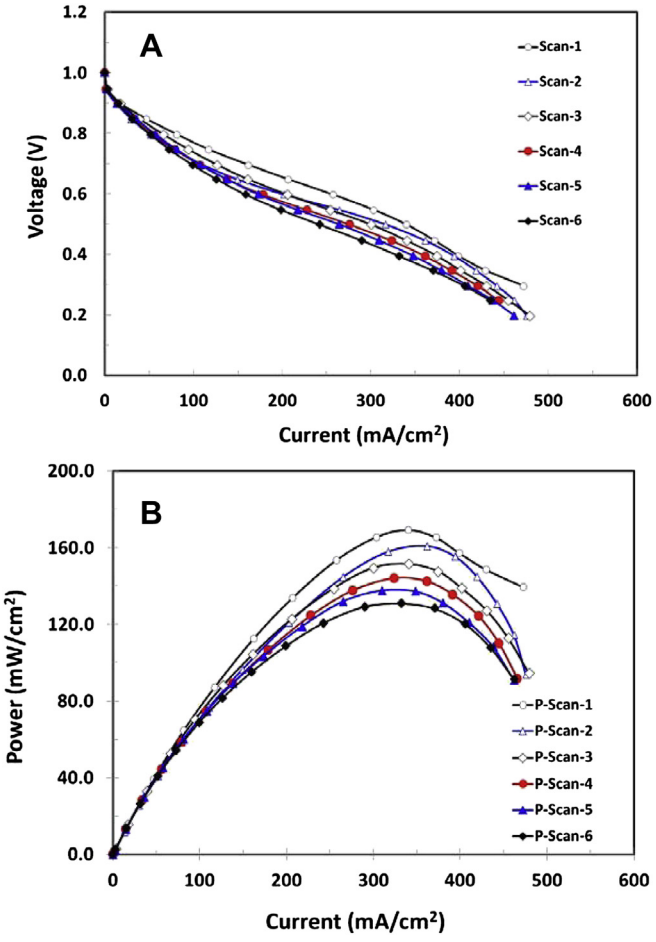

Fig. 10. Voltage–current (A) and power-current (B) curves of a single H_2/O_2 cell using 40% Pt/C as both the cathode and anode catalyst, Tokuyama A201 (alkaline) as the electrolyte membrane (KOH free), and an operating temperature of 60 °C.

4. Conclusion

The catalyst $CoFeN_x/C$, obtained by pyrolysis of hemin from porcine and 5,10,15,20-tetrakis(4-methoxyphenyl)-21*H*,23*H*-porphine cobalt(II) (CoTMPP), showed high catalytic activity for the 4-electron reduction of oxygen to water through a synergetic process. First, a 2-electron reduction of oxygen to H_2O_2 at the cobalt sites occurs followed by the reduction of H_2O_2 to water at the iron sites. The overall reaction yields a 4-electron reduction of oxygen. Comparative analyses of catalytic kinetic processes of oxygen reduction in acidic and alkaline electrolytes were also conducted with RDE and RRDE methods. In an alkaline electrolyte, a larger electron transfer coefficient was obtained (0.63), signifying a larger fraction of the interfacial potential at the electrode/KOH electrolyte interface. This helps lower the free energy barrier for oxygen reduction in KOH solution. The kinetic rate for catalytic oxygen reduction in alkaline solution at 0.6 V (versus RHE) is almost 4 times higher than that in acidic solution. The $CoFeN_x/C$ catalyst was further evaluated as a cathode catalyst in single fuel cells with acidic, neutral and alkaline electrolyte membranes. The order of the single fuel cell performances was determined to be acidic > neural > alkaline, which is in the opposite order of the half cell performance in alkaline and acidic electrolytes. This phenomenon is attributed to unstable alkaline electrolyte membrane in KOH-free operating conditions. This result indicates that a good non-noble metal catalyst must match a suitable electrolyte membrane for practical fuel cell applications.

Acknowledgments

The authors would like to thank the U.S. Department of the Army and U.S. Army Materiel Command for support to this work, and Dr. Cynthia Lundgren and Dr. Kyle N. Grew for review and helpful discussions.

References

[1] J.R. Varcoe, R.C.T. Slad, Fuel Cells 5 (2) (2005) 187.
[2] C.C. Yang, J. Appl. Electrochem. 42 (2012) 305.
[3] Y.T. Luo, J.C. Guo, C.S. Wang, D. Chu, Electrochem. Commun. 16 (2012) 65.
[4] Y.S. Li, T.S. Zhao, Z.X. Liang, J. Power Sources 187 (2009) 387.
[5] E.E. Switzer, T.S. Olson, A.K. Datye, P. Atanassov, M.R. Hibbs, C. Fujimoto, C.J. Cornelius, Electrochim. Acta 55 (2010) 3404.
[6] M. Schulze, E. Gulzow, G. Steinhilber, Appl. Surf. Sci. 179 (2001) 251.
[7] J.P. Shim, Y.S. Park, H.K. Lee, J.S. Lee, J. Power Sources 74 (1998) 151.
[8] X.H. Wang, Y. Chen, H.G. Pan, R.G. Xu, S.Q. Li, L.X. Chen, C.P. Chen, Q.D. Wang, J. Alloys Compd. 293–295 (1999) 833.
[9] M. Schulze, E. Gulzow, J. Power Sources 127 (2004) 252.
[10] J.A.R. van Veen, H.A. Colijn, J.F. van Baar, Electrochim. Acta 33 (6) (1988) 801.
[11] S.J. Dong, R.Z. Jiang, Ber. Bunsenges. Phys. Chem. 91 (4) (1987) 479.
[12] S.L. Gojkovic, S. Gupta, R.F. Savinell, J. Electroanal. Chem. 462 (1) (1999) 63.
[13] R.Z. Jiang, D. Chu, J. Electrochem. Soc. 147 (12) (2000) 4605.
[14] R.Z. Jiang, D.T. Tran, J. McClure, D. Chu, Electrochem. Commun. 19 (2012) 73.
[15] R.Z. Jiang, D.T. Tran, J. McClure, D. Chu, Electrochim. Acta 75 (2012) 185.
[16] J.L. Oberst, M.S. Thorum, A.A. Gewirth, J. Phys. Chem. C 116 (2012) 25257.
[17] R.R. Chen, H.X. Li, D. Chu, G.F. Wang, J. Phys. Chem. C 113 (2009) 20689.
[18] C.W.B. Bezerra, L. Zhang, K.C. Lee, H.S. Liu, A.L.B. Marques, E.P. Marques, H.J. Wang, J.J. Zhang, Electrochim. Acta 53 (2008) 4937.
[19] A.V. Palenzuela, L. Zhang, L.C. Wang, P.L. Cabot, E. Brillas, K. Tsay, J.J. Zhang, J. Phys. Chem. C 115 (2011) 12929.
[20] A.V. Palenzuela, L. Zhang, L.C. Wang, P.L. Cabot, E. Brillas, K. Tsaya, J.J. Zhang, Electrochim. Acta 56 (2011) 4744.
[21] G. Wu, M. Nelson, S.G. Ma, H. Meng, G.F. Cui, P.K. Shen, Carbon 49 (2011) 3972.
[22] L. Zhang, K.C. Lee, C.W.B. Bezerra, J.L. Zhang, J.J. Zhang, Electrochim. Acta 54 (2009) 6631.
[23] A. Videla, L. Zhang, J. Kim, J. Zeng, C. Francia, J.J. Zhang, S. Specchia, J. Appl. Electrochem. 43 (2013) 159.
[24] J.Y. Choi, R.S. Hsu, Z.W. Chen, J. Phys. Chem. C 114 (2010) 8048.
[25] H.R. Byon, J. Suntivich, S.H. Yang, Chem. Mater. 23 (2011) 3421.
[26] T. Schilling, M. Bron, Electrochim. Acta 53 (2008) 5379.
[27] S.L. Gojkovk, S. Gupta, R.F. Savinell, J. Electrochem. Soc. 145 (1998) 3494.
[28] J.D.W. Camacho, K.J. Stevenson, J. Phys. Chem. C 115 (2011) 20002.
[29] E.B. Yeager, Electrochim. Acta 29 (1984) 1527.
[30] R.R. Durand, C.S. Bencosme, J.P. Collman, F.C. Anson, J. Am. Chem. Soc. 105 (1983) 2710.
[31] D. Chu, R.Z. Jiang, Solid State Ionics 148 (3–-4) (2002) 591.
[32] R.Z. Jiang, F.C. Anson, J. Electroanal. Chem. 305 (1991) 171.
[33] R.N. Itoe, G.D. Wesson, E.E. Kalu, J. Electrochem. Soc. 147 (2000) 2445.
[34] R.Z. Jiang, S.J. Dong, J. Electroanal. Chem. 246 (1988) 101.